Journal Geophysical Research -Solid Earth

Supporting Information for

Subduction-induced upwelling of a hydrous transition zone: Implications for the Cenozoic magmatism in Northeast China

Lin Chen[1], Manuele Faccenda[2,*]

[1] *State Key Laboratory of Lithospheric Evolution, Institute of Geology and Geophysics, Chinese Academy of Sciences, Beijing 100029, China*

[2] *Dipartimento di Geoscienze, Università di Padova, 35131 Padova, Italy*

[*] *Corresponding author*

Contents of this file

Introduction

Here we explain more in detail the fundamental equations behind the thermo-mechanical modeling (Text S1) and the rheological model (Text S2, Table S1). Furthermore, we provide the equations used to parametrize the melting curves of peridotite in presence of water (Text S3) and 3 additional Figures S1-3 showing the evolution of models Sta7-9.

Text S1. Fundamental equations

The momentum, continuity, and thermal equations for the two-dimensional creeping-flow, accounting for thermal and chemical buoyancy, are solved using the I2VIS code [*Gerya and Yuen*, 2003] based on conservative finite differences and a non-diffusive marker-in-cell technique.

The thermal equations for conservation of heat have the form:

$$\rho(\mathrm{P,T,C,M})\mathrm{C_p}\left(\frac{\mathrm{DT}}{\mathrm{Dt}}\right) = -\frac{\partial \mathrm{q_x}}{\partial \mathrm{x}} - \frac{\partial \mathrm{q_z}}{\partial \mathrm{z}} + \mathrm{H_r} + \mathrm{H_a} + \mathrm{H_s} + \mathrm{H_L} \qquad \text{(A1)}$$

$$\mathrm{q_x} = -\mathrm{k(T,P,C)}\frac{\partial \mathrm{T}}{\partial \mathrm{x}},\ \mathrm{q_z} = -\mathrm{k(T,P,C)}\frac{\partial \mathrm{T}}{\partial \mathrm{z}}$$

$$\mathrm{H_a} = \mathrm{T}\alpha\frac{\mathrm{DP}}{\mathrm{Dt}},\ \mathrm{H_s} = \sigma'_{xx}\dot{\varepsilon}_{xx} + \sigma'_{\mathrm{zz}}\dot{\varepsilon}_{zz} + 2\sigma'_{\mathrm{xz}}\dot{\varepsilon}_{xz}$$

where $\mathrm{D/Dt}$ is the substantive time derivative; x and z denote the horizontal and vertical coordinates; σ'_{xx}, σ'_{xz}, σ'_{xz} are the components of the deviatoric stress tensor, while $\dot{\varepsilon}_{xx}$, $\dot{\varepsilon}_{xz}$, $\dot{\varepsilon}_{zz}$ are the components of the strain rate tensor; ρ is the density as a function of pressure (P), temperature (T), composition (C) and melt fraction (M); $\mathrm{q_x}$ and $\mathrm{q_z}$ are heat flux components; $\mathrm{k(T,P,C)}$ is the thermal conductivity; $\mathrm{C_p}$ is the isobaric heat capacity; α is the thermal expansion; $\mathrm{H_r}$, $\mathrm{H_a}$, $\mathrm{H_s}$, $\mathrm{H_L}$, respectively, are radioactive, adiabatic, shear and latent heat production.

The conservation of mass is approximated by the incompressible continuity equation:

$$\frac{\partial \mathrm{v_x}}{\partial \mathrm{x}} + \frac{\partial \mathrm{v_z}}{\partial \mathrm{z}} = 0 \qquad \text{(A2)}$$

where $\mathrm{v_x}$ and $\mathrm{v_z}$ are the horizontal and vertical components of the velocity vector, respectively.

The 2D Stokes equations for conservation of momentum take the form:

$$\frac{\partial \sigma'_{xx}}{\partial \mathrm{x}} + \frac{\partial \sigma'_{xz}}{\partial \mathrm{z}} = \frac{\partial \mathrm{P}}{\partial \mathrm{x}} \qquad \text{(A3)}$$

$$\frac{\partial \sigma'_{zz}}{\partial \mathrm{z}} + \frac{\partial \sigma'_{xz}}{\partial \mathrm{x}} = \frac{\partial \mathrm{P}}{\partial \mathrm{z}} - \mathrm{g}_y\rho(\mathrm{P,T,C,M}) \qquad \text{(A4)}$$

where g_y is the vertical component of the gravitational acceleration.

The deviatoric stress tensor σ'_{ij} relates to effective viscosity η_{eff} and the strain rate tensor $\dot{\varepsilon}_{ij}$ via:

$$\sigma'_{ij} = 2\eta_{eff}\dot{\varepsilon}_{ij} \quad \text{(A5)}$$

$$\dot{\varepsilon}_{ij} = \frac{1}{2}\left(\frac{\partial v_i}{\partial x_j} + \frac{\partial v_j}{\partial x_i}\right) \quad \text{(A6)}$$

Text S2. Rheological model

The strength of the lithosphere is controlled, on the geologic timescale, by the combination of both brittle and ductile deformation mechanisms. The brittle part of the lithosphere is controlled by the Drucker-Prager plasticity which expresses the linear dependence of the materials resistance on the total pressure. The yield criterion is implemented as follows [*Gerya*, 2010a]:

$$\sigma_{yield} = C + Psin(\varphi_{eff}) \quad \text{(A7)}$$

$$sin(\varphi_{eff}) = sin(\varphi)(1\text{-}\lambda_{\text{fluid}}) \quad \text{(A8)}$$

$$\lambda_{\text{fluid}} = \frac{P_{\text{fluid}}}{P_{\text{total}}} \quad \text{(A9)}$$

$$\eta_{plastic} = \frac{\sigma_{yield}}{2\dot{\varepsilon}_{II}} \quad \text{(A10)}$$

where σ_{yield} is the yield stress; P is the total dynamic pressure; C is the cohesion at $P = 0$; φ is the internal frictional angle; λ_{fluid} is the pore fluid pressure factor that reduces the yield strength of fluid-containing porous or fractured rocks; $\dot{\varepsilon}_{II} = \left(0.5\dot{\varepsilon}_{ij}\dot{\varepsilon}_{ij}\right)^{1/2}$ is the second invariant of the strain rate tensor; $\eta_{plastic}$ is the viscosity for plastic rheology. φ_{eff} can be illustrated as the effective internal frictional angle that integrates the effects of internal frictional angle and pore fluid coefficient.

We assume that the plastic strength of fractured rocks is significantly reduced by percolating fluids and high pore fluid pressure. Strain weakening associated fracturing is implemented as follows [*Huismans and Beaumont*, 2002; *Gerya*, 2010b]:

$$C = \begin{cases} C_a + (C_b - C_a) \times \frac{\gamma}{\gamma_{cr}}, & \text{if } \gamma \leq \gamma_{cr} \\ C_b, & \text{if } \gamma > \gamma_{cr} \end{cases} \quad \text{(A11)}$$

$$\varphi = \begin{cases} \varphi_a + (\varphi_b - \varphi_a) \times \frac{\gamma}{\gamma_{cr}}, & \text{if } \gamma \leq \gamma_{cr} \\ \varphi_b, & \text{if } \gamma > \gamma_{cr} \end{cases} \quad \text{(A12)}$$

where γ is the integrated plastic strain and γ_{cr} is the upper limit of strain for fracture-related weakening; C_a and φ_a are the initial frictional angle and cohesion; C_b and φ_b are the final frictional angle and cohesion.

The viscosity for ductile creep is given by [*Ranalli*, 1995]:

$$\eta_{ductile} = (\dot{\varepsilon}_{II})^{(1-n)/n} \eta_0{}^{-1/n} exp\left(\frac{E_a + PV_a}{nRT}\right) \quad \text{(A13)}$$

where η_0 (material constant), E_a (activation energy), V_a (activation volume), n (stress exponent) are experimentally determined flow law parameters. R is the gas constant and T is the absolute temperature.

The final visco-plastic rheology is determined by comparing brittle/plastic and creep viscosities as a function of depth [*Ranalli*, 1995]:

$$\eta = min\{\eta_{plastic}, \eta_{ductile}\} \quad \text{(A14)}$$

In the modeling, we use the experimentally-determined flow law of 'wet quartzite' for the continental upper crust, 'plagioclase An75' for the continental lower crust, and 'dry (wet) olivine' for the dry (wet) lithospheric and asthenospheric mantle [*Ranalli*, 1995]. A lower cut-off value of 10^{18} Pa s and an upper cut-off value of 10^{26} Pa s are applied for viscosity of all types of rocks in our numerical experiments. A lower cut-off value of 10^{17} Pa s is assigned to all partially molten rocks to further reduce the effective viscosity [*Pinkerton and Stevenson*, 1992], ensuring a large viscosity contrast with the surrounding subsolidus mantle. The rheological parameters used in this study are listed in Table S1.

Text S3. Melting conditions for the mantle rocks with varying water content (compiled from Litasov [2011])

Water saturated solidus (T_{ssat}) is given by:

When $P \leq 1.54\ GPa$,

$$T_{ssat} = 1172.64 - 491.60 * P + 396.12 * P^2 - 103.23 * P^3 \quad \text{(A15)}$$

When $1.54 < P \leq 9.50\ GPa$,

$$T_{ssat} = 923.15 + 43.36 * P - 6.08 * P^2 + 0.28 * P^3 \quad \text{(A16)}$$

When $9.50 < P \leq 12.68\ GPa$,

$$T_{ssat} = 594.52 + 45.20 * P \quad \text{(A17)}$$

When $12.68 < P \leq 16.48\ GPa$,

$$T_{ssat} = 2510.66 - 301.73 * P + 23.50 * P^2 - 0.66 * P^3 \quad \text{(A18)}$$

When $P > 16.48\ GPa$,

$$T_{ssat} = -1081.94 + 216.36 * P - 6.43 * P^2 + 0.08 * P^3 \quad \text{(A19)}$$

where P is pressure in GPa and T is temperature in Celsius (the same below).

For zero water content (wa) case, the solidus (T_s) is given by:

When $P \leq 2.17\ GPa$,

$$T_s = 1151.21 + 36.09 * P + 71.02 * P^2 - 16.74 * P^3 \quad \text{(A20)}$$

When $P > 2.17\ GPa$,

$$T_s = 1103.54 + 155.99 * P - 10.66 * P^2 + 0.40 * P^3 - 0.0061 * P^4 \quad \text{(A21)}$$

For $wa = 0.01$ wt%, the solidus is given by:

When $P \leq 14.87\ GPa$,

$$T_s = 689.32 + 221.92 * P - 13.87 * P^2 + 0.33 * P^3 \quad \text{(A22)}$$

When $14.87 < P \leq 15.17\ GPa$,

$$T_s = 457.74 + 105.11 * P \quad \text{(A23)}$$

When $P > 15.17\ GPa$,

$$T_s = 2199.24 - 35.45 * P + 2.29 * P^2 - 0.038 * P^3 \quad \text{(A24)}$$

For $wa = 0.05$ wt%, the solidus is given by:

When $P \leq 4.76\ GPa$,

$$T_s = 789.09 + 93.51 * P \quad \text{(A25)}$$

When $4.76 < P \leq 14.63\ GPa$,

$T_s = -100.97 + 409.08 * P - 31.08 * P^2 + 0.86 * P^3$ (A26)

When $14.63 < P \leq 15.02\ GPa$,

$T_s = -556.66 + 168.18 * P$ (A27)

When $P > 15.02\ GPa$,

$T_s = 1888.06 + 5.31 * P$ (A28)

For $wa = 0.1$ wt%, the solidus is given by:

When $P \leq 6.73\ GPa$,

$T_s = 689.00 + 231.20 * P - 56.13 * P^2 + 5.25 * P^3$ (A29)

When $6.73 < P \leq 13.94\ GPa$,

$T_s = -947.89 + 612.16 * P - 51.31 * P^2 + 1.49 * P^3$ (A30)

When $13.94 < P \leq 14.87\ GPa$,

$T_s = -835.53 + 179.01 * P$ (A31)

When $P > 14.87\ GPa$,

$T_s = 1821.36 + 0.70 * P$ (A32)

For $wa = 0.5$ wt%, the solidus is given by:

When $P \leq 13.11\ GPa$,

$T_s = -27012.30 + 6778.70 * P - 542.36 * P^2 + 14.51 * P^3$ (A33)

When $13.11 < P \leq 14.19\ GPa$,

$T_s = -62854.39 + 14314.28 * P - 1074.53 * P^2 + 27.16 * P^3$ (A34)

When $P > 14.19\ GPa$,

$T_s = 1505.18 + 0.75 * P$ (A35)

For $wa > 0.5$ wt%, the solidus is given by:

$T_s = T_{ssat}$

For the mantle rock with a water content between wa_1 and wa_2, the solidus at a given P is defined as:

$T_s = T_{s\_wa1} - \left(T_{s\_wa1} - T_{s\_wa2}\right) * (wa - wa_1)/(wa_2 - wa_1)$ (A36)

where $T_{s\_wa1} > T_{s\_wa2}$ are solidus with $wa = wa_1$ and $wa = wa_2 > wa_1$, respectively.

Liquidus (T_l) for mantle rocks is given by:

When $P \leq 13.67\ GPa$,

$T_l = 1698.11 + 56.12 * P - 1.97 * P^2 + 0.01 * P^3$ (A37)

When $P > 13.67\ GPa$,

$$T_l = 1720.23 + 29.44 * P \quad \text{(A38)}$$

References

Gerya, T., Yuen, D., 2003. Characteristics-based marker-in-cell method with conservative finite-differences schemes for modeling geological flows with strongly variable transport properties. Phys. Earth Planet. Inter.140 (4), 293–318.

Gerya, T., 2010a. Introduction to Numerical Geodynamic Modelling. Cambridge University Press.

Gerya, T., 2010b. Dynamical instability produces transform faults at mid-ocean ridges. Science 329 (5995), 1047–1050.

Huismans, R.S., Beaumont, C., 2002. Asymmetric lithospheric extension: the role of frictional plastic strain softening inferred from numerical experiments. Geology30 (3), 211–214.

Iwamori, H., 2004. Phase relations of peridotites under H_2O-saturated conditions and ability of subducting plates for transportation of H_2O. Earth Planet. Sci. Lett. 227, 57-71.

Litasov, K.D., 2011. Physicochemical conditions for melting in the Earth's mantle containing a C-O-H fluid (from experimental data). Russian Geology and Geophysics 52, 475-492.

Litasov, K.D., Shatskiy, A., Ohtani, E., 2014. Melting and subsolidus phase relations in peridotite and eclogite systems with reduced C-O-H fluid at 3-16 GPa. Earth Planet. Sci. Lett. 391, 87-99.

Pinkerton, H., Stevenson, R.J., 1992. Methods of determining the rheological properties of magmas at subliquidus temperatures. J. Volcanol. Geotherm. Res. 53, 47–66.

Ranalli, G., 1995. Rheology of the Earth, Deformation and Flow Processes in Geophysics and Geodynamics, seconded. Chapman & Hall., p.334.

Supplementary Figures

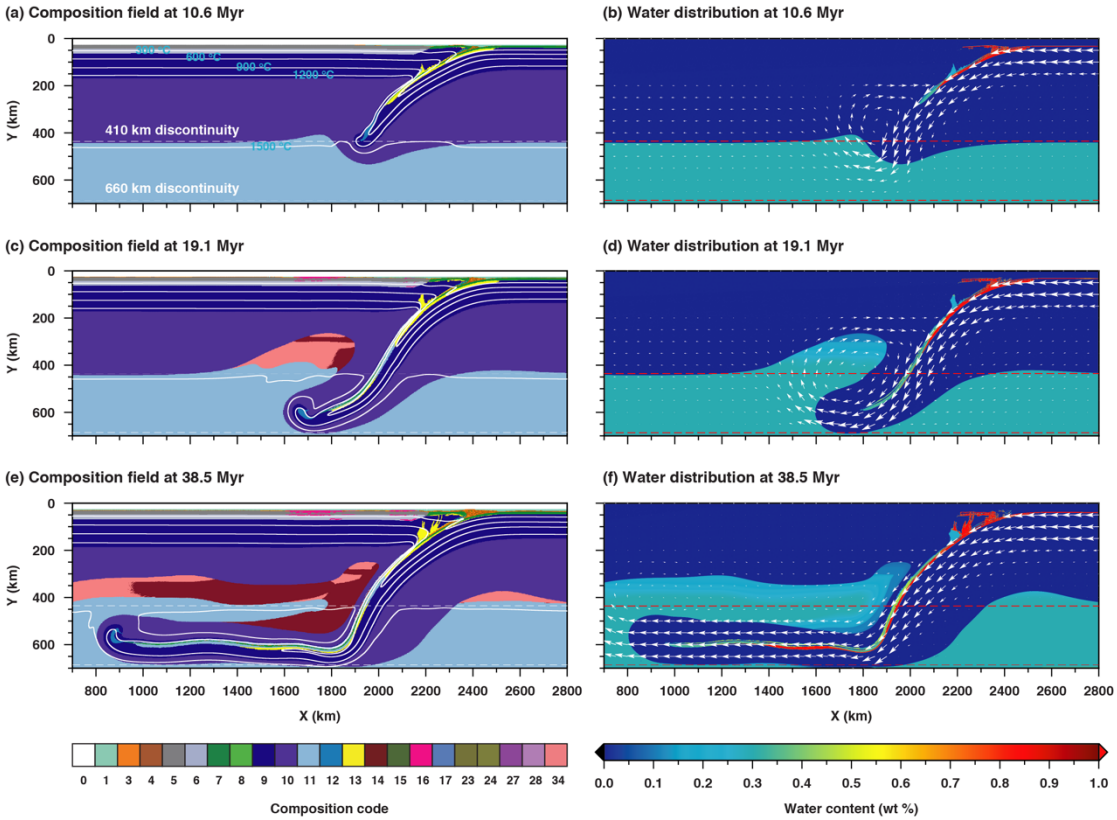

Figure S1. **Time evolution of the model 'Sta7' (Table 1). This model is identical to the reference model except that it has a younger slab (40 Ma). The left column shows the temporal evolution of the compositional field, while the right column shows the corresponding evolution of the water distribution. White lines overprinted on the composition fields show isotherms with an interval of 300 °C (the same below). White arrows indicate the motion of the material. Dashed lines outline the unperturbed TZ. Composition codes: 0, sticky air; 1, sea water; 3 and 4, sediment; 5, upper continental crust; 6, lower continental crust; 7, upper oceanic crust; 8, lower oceanic crust; 9, lithospheric mantle; 10, asthenospheric mantle; 11, hydrated mantle; 12, weak zone; 13, serpentinized mantle; 14, recrystallized (previously partially molten) mantle; 15, lower mantle; 16, extracted molten basalt; 17, extracted molten sediment or upper continental crust; 23-24, partially molten sediment; 27, partially molten basalt; 28, partially molten gabbro; 34, partially molten wet peridotite.**

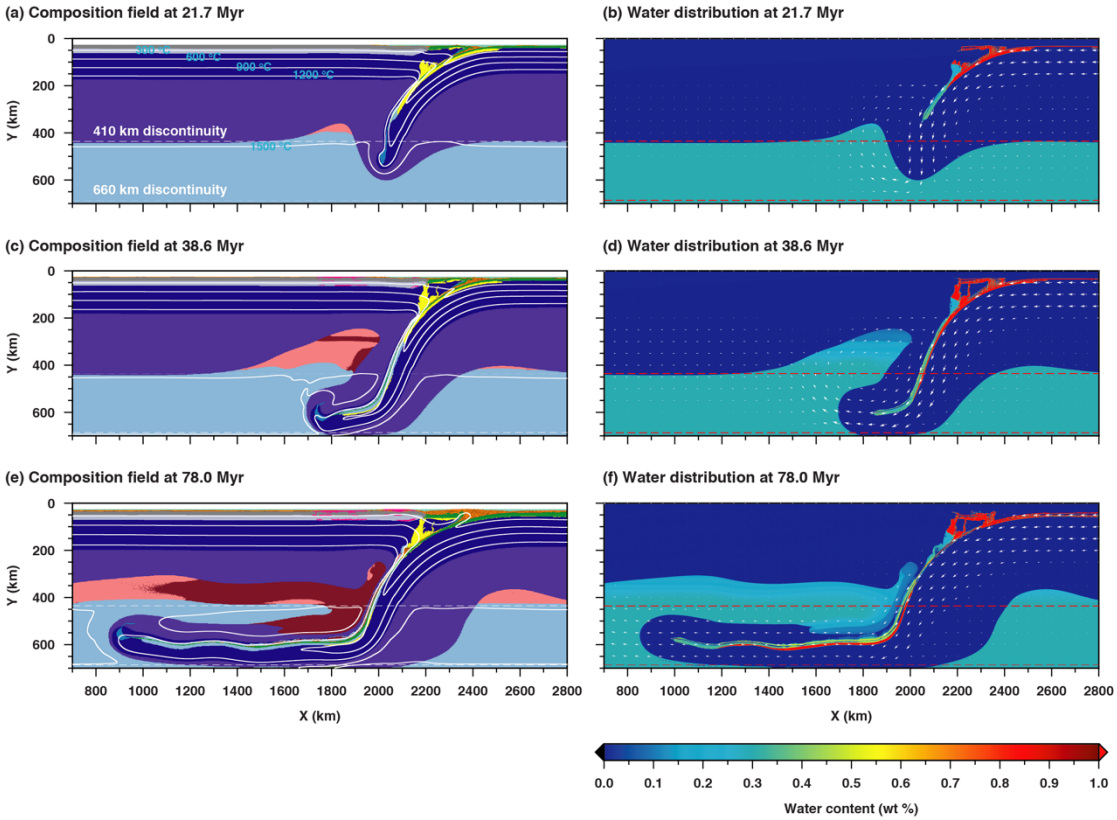

Figure S2. **Time evolution of the model 'Sta8' (Table 1). This model is identical to the reference model except that it has a slower convergence rate (2.5 cm/yr). The left column shows the temporal evolution of the compositional field, while the right column shows the corresponding evolution of the water distribution. White arrows indicate the motion of the material. Dashed lines outline the unperturbed TZ. See FigureS1 for composition code.**

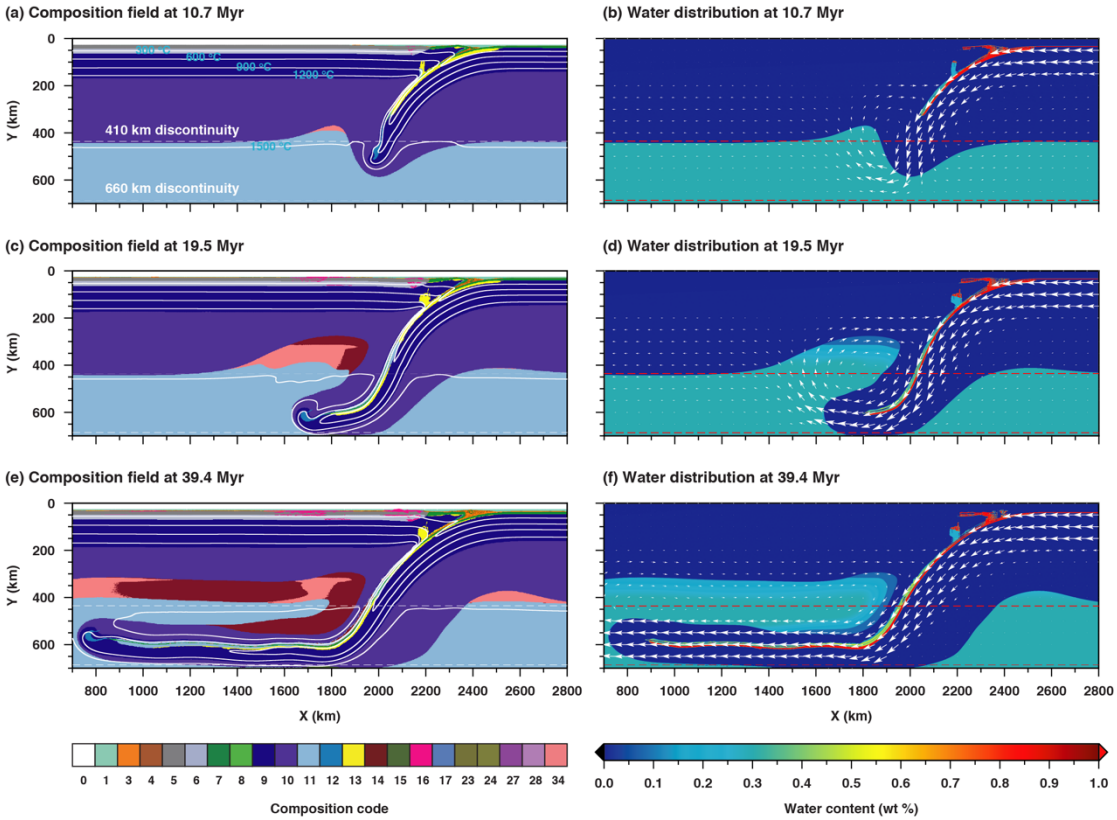

Figure S3. **Time evolution of the model 'Sta9' (Table 1). This model is identical to the reference model except that it has a smaller minimum threshold of melt fraction for melt extraction ($M_{min} = 2\%$). The left column shows the temporal evolution of the compositional field, while the right column shows the corresponding evolution of the water distribution. White arrows indicate the motion of the material. Dashed lines outline the unperturbed TZ. See FigureS1 for composition code.**

Table S1 Rheological parameters of material used in this study (Ranalli, 1995) [a]

Material	Flow law	η_0 (Pa^n S)	n	E_a (J)	V_a (J/bar)	$\sin(\varphi)$	C (MPa)
Stick air	N.A.	1.00×10^{19}	-	-	-	-	-
Water	N.A.	1.00×10^{19}	-	-	-	-	-
Sediment	W.Q.	1.97×10^{17}	2.3	1.54×10^{5}	0.8	0.05	1
UCC	W.Q.	1.97×10^{17}	2.3	1.54×10^{5}	0.8	0.2-0.1	1
LCC	PL.	4.80×10^{22}	3.2	2.38×10^{5}	1.0	0.15	1
UOC	PL.	4.80×10^{22}	3.2	2.38×10^{5}	0.8	0.05	1
LOC	PL.	4.80×10^{22}	3.2	2.38×10^{5}	1.0	0.15	1
LM	D.O.	3.98×10^{16}	3.5	5.32×10^{5}	1.2	0.6-0.4	1
AM	D.O.	3.98×10^{16}	3.5	5.32×10^{5}	1.2	0.6-0.4	1
RM	D.O.	3.98×10^{16}	3.5	5.32×10^{5}	1.2	0.6-0.4	1
HM	W.O.	5.01×10^{20}	4.0	4.70×10^{5}	1.2	0.6-0.4	1
SM	W.O.	5.01×10^{20}	4.0	4.70×10^{5}	1.2	0.6-0.4	1
WZ	W.O.	5.01×10^{20}	4.0	4.70×10^{5}	1.2	0	1
LOM	D.O.	3.98×10^{16}	3.5	5.32×10^{5}	1.2	0.6-0.4	1
EMB	PL.	4.80×10^{22}	3.2	2.38×10^{5}	1.0	0.15	1
EMS	W.Q.	1.97×10^{17}	2.3	1.54×10^{5}	1.0	0.2-0.1	1
PMS	W.Q.	1.97×10^{17}	2.3	1.54×10^{5}	0.8	0.06	0
PMB	PL.	4.80×10^{22}	3.2	2.38×10^{5}	0.8	0.15	0
PMG	PL.	4.80×10^{22}	3.2	2.38×10^{5}	1.0	0.15	0
PMWP	W.O.	5.01×10^{20}	4.0	4.70×10^{5}	1.2	0.2	0

[a] η_0 is the pre-exponential constant; n is the stress exponent; E_a is the activation energy; V_a is the activation volume; φ is the friction angle; C is the cohesion. For material: UCC, upper continental crust; LCC, lower continental crust; UOC, upper oceanic crust (basalt); LOC, lower oceanic crust (gabbro); LM, lithospheric mantle; AM, asthenospheric mantle; RM, recrystallized mantle; HM, hydrated mantle; SM,

serpentinized mantle; WZ, weak zone; LOM, lower mantle; EMB, extracted molten basalt; EMS, extracted molten sediment or upper continental crust; PMS, partially molten sediment; PMB, partially molten basalt; PMG, partially molten gabbro; PMWP, partially molten wet peridotite. For flow law: N.A., not applicable; W.Q., wet quartz; PL., plagioclase (An75); D.O., dry olivine; W.O., wet olivine.